Analysis and Optimization of Dysprosium-Doped Yellow Fiber Lasers for Ophthalmology Applications

Foroogh Khozeymeh, Federica Poli, *Member, IEEE*, Wahida Chowdhury, and Annamaria Cucinotta, *Senior Member, IEEE*

***Abstract*—In this paper, a Forward Time Centered Space (FTCS) method and an analytical method have been developed to fully investigate the $^4F_{9/2}$ to $^6H_{13/2}$ lasing transition of a dysprosium Dy−doped ZBLAN fiber which provides the potential of highly efficient yellow laser direct generation. This light source is of significant interest for treating diabetic retinopathy, which can cause blindness. The developed method's validity is confirmed through the comparison with experimental investigations of Dy−doped ZBLAN fiber lasers in other valid research. A full analysis of Dy−doped fiber laser including the population of the energy levels, power evolution of the laser and pump signals, amplified spontaneous emission (ASE), excited state absorption (ESA), radiative and non-radiative time transition rates are presented. The developed numerical method gives a better understanding of the impact of ASE and ESA on laser performance. The influence of overlap integrals, output mirror reflectivity, and active fiber length on laser performance is investigated. The optimization criteria based on the different robust configurations of laser cavities are found which predict the slope efficiencies higher than half of the Stokes limit.**

***Index Terms*—Diabetic retinopathy, fiber laser, FTCS method, slope efficiency.**

I. Introduction

YELLOW fiber-based lasers emitting around 565–590 nm are of particular interest for their existing and potential applications in sodium laser guide star [1], ophthalmology [2], and in particular medical treatment for diabetic retinopathy (DR) [3], and optical clock [4]. DR is the most common eye disease among diabetic patients which causes vision impairment and blindness. In the treatment of DR, experimental investigations on animals and humans, but also numerical analysis, have confirmed that yellow laser emission is the most suitable candidate, because it is effective with low power, and presents good clinical results with minimal collateral effects [3], [5], [6]. So far yellow emission has been possible with several techniques from copper bromide laser [7], Yb−doped fiber [8], bi − fiber lasers [9], optically pumped semiconductor lasers [10]. However, these techniques demand bulky structures with a number of free-space alignments, high maintenance, and tight limitations on the pump conditions. For accessing high-efficiency and simple direct yellow laser emission, particularly Dy−doped ZBLAN fiber lasers, exploiting transition of $^4F_{9/2}$ to $^6H_{13/2}$, are desirable candidates. Therefore, the design, modeling, and fabrication of compact and efficient Dy−doped yellow fiber lasers are critically important.

Dysprosium is a rare earth element that, depending on the pumping scheme, can be used for the generation of coherent radiation not only in yellow [11] but also in the mid-infrared (Mid-IR) range, as it is demonstrated by the Dy-doped chalcogenide glass high-efficiency master oscillator power amplifier in [12] or the novel Dy $^{3+}$: Ga_5 Ge_{20} Sb_{10} S_{65} fiber laser in [13]. Very recently a Dy−doped silica fiber has been employed as a saturable absorber for Mid-IR pulsed all-fiber lasers [14].

Regarding the development path of Dy−doped ZBLAN materials for yellow emission, in 2001 [11], the first CW yellow emission in a Dy−doped ZBLAN fiber laser was demonstrated. Although Dy−doped yellow fiber lasers have been analyzed in some other research works [15], [16], [17], still the reported slope efficiencies were less than 13.2%. Indeed, in a considerable time period, due to the lack of high-performance gain fibers and high-power GaN blue lasers as the pumping sources, no significant research progress has been observed in Dy−doped fiber yellow lasers. In 2020, thanks to the breakthroughs of both Dy−doped fluoride fibers and high-power blue GaN laser diodes, the first Dy−doped ZBLAN fiber laser pumped by GaN laser diode, emitting at 445 nm, was reported [18]. By employing ZBLAN fluoride fibers for obtaining the yellow emission, in [18], the maximum laser slope efficiency of 2.3% and 0.9% was reported in a Dy−doped fiber with lengths of 0.6 m and 5.95 m respectively. In 2021, the same researchers investigated the potential causes of the low experimental slope efficiency. They found contributions from the background loss of the fiber and excited-state absorption (ESA) of the intracavity yellow light [19]. They measured a maximum slope efficiency of 33% [19], which is still less than half of the Stokes limit, which is about 78%. Notice that the Stokes limit (λ_p/λ_s), is defined as the ratio of the pump wavelength (λ_p), to signal or laser wavelength (λ_s). Recently, Dy−doped multi-component phosphate glass was examined and showed a strong yellow emission which was due to the high asymmetry and covalency of the local field and the high phonon energy [20]. In that work, Dy−doped multi-component phosphate core glass fiber was successfully drawn by using a rod-in-tube method. Fluoride fibers have been

Manuscript received 24 October 2023; revised 27 November 2023; accepted 30 November 2023. Date of publication 5 December 2023; date of current version 26 December 2023. This work was supported by PRIN 2020 MUR "*Yellow Fiber Laser System for the treatment of oCular disEases (Yellow-FLiCkEr)*" - ERC Sector PE7. *(Corresponding author: Annamaria Cucinotta.)*

The authors are with the Department of Engineering and Architecture, University of Parma, 43124 Parma, Italy (e-mail: foroogh.khozeymehsarbishe@unipr.it; annamaria.cucinotta@unipr.it).

Digital Object Identifier 10.1109/JPHOT.2023.3339595

recently employed to build novel Mid-IR sources as well [21], [22]. Furthermore, in [23], another Dy−doped $NaLa(WO_4)_2$ glass ceramic fiber with good uniformity was fabricated using the molten core method showing that it can be a very promising material candidate for tunable yellow lasers [23]. Despite these positive results in the fabrication technology of new glasses, the most promising commercially available Dy−doped ZBLAN fiber is the one produced by Le Verre Fluoré, France [24]. On the other hand, despite the interesting results obtained with this fiber [18], [19], [25], the maximum reported slope efficiency is still only about half of the Stokes limit. Until now, few research works have dealt fully with the causes of the low slope efficiency in Dy−doped fiber yellow lasers. Therefore, it is necessary to propose more numerical and analytical methods for further improvements in the performance of Dy−doped ZBLAN fiber lasers.

In this paper, we have used a Forward Time Centered Space (FTCS) method [26] and analytical methods for deep analysis and further understanding of Dy−doped ZBLAN fiber laser properties. This has led us to obtain a suitable and comprehensive model which figures out the impact of different physical parameters such as pump and signal overlap integrals with the doped region, as well as cavity parameters (active fiber length and mirror's reflectivity), on laser output performance. On the other hand, the developed numerical method has assessed the impact of both ESA and amplified spontaneous emission (ASE) on the output power of the laser. Finally, the optimization criteria providing high slope efficiency (more than half of the Stokes limit) lasers, have been found. This in turn will pave the way for design, modeling, and employing the high slope efficiency Dy−doped ZBLAN fiber lasers in DR treatments.

II. Dy−doped Fiber Laser

A Dy−doped ZBLAN fiber with the same structural parameters as the one made by Le Verre Fluoré, France [24] (doping concentration of 0.2 mol. %, core diameter of 12.5 μm, and numerical aperture of 0.16) is considered. The energy level schematic of Dy^{3+} ion for yellow fluorescence emission is shown in Fig. 1. As it has been mentioned the ${}^4F_{9/2} \rightarrow {}^6H_{13/2}$ energy transition, produces strong yellow fluorescence around 573 nm. This lasing can be obtained by pumping from the ground state level (${}^6H_{15/2}$) to the ${}^4I_{15/2}$ level by a shorter wavelength in the blue range (450 nm). Then non-radiative transition (shown by the rate of $A_{32} = 1/\tau_{32}$ in Fig. 1) will produce a population inversion between the higher lasing level of ${}^4F_{9/2}$ and the lower lasing level of ${}^6H_{13/2}$. Once the yellow emission is produced by ${}^4F_{9/2} \rightarrow {}^6H_{13/2}$ energy transition, there is a possibility of yellow light re-absorption (as shown by the upward dashed line in Fig. 1). This is due to the comparable lifetime of the lower laser level which is 0.65 ms and of the upper laser level which is 1.5 ms. Hence, a massive population accumulates on the lower laser level, which can subsequently re-absorb the yellow light. Additionally, $A_{30} = 1/\tau_{30}$ shows the spontaneous decay rate at the pump wavelength. Finally, the amplified spontaneous emission rate from the upper to the lower lasing level $A_{21}(\lambda_s)$, has been also taken into account.

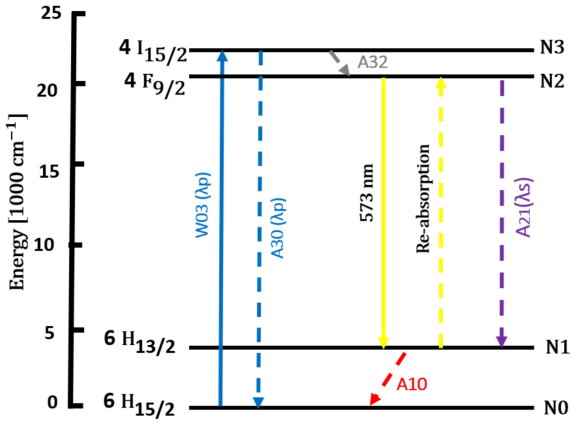

Fig. 1. Simplified Dy^{3+} energy level diagram showing ground-state absorption (GSA) for ~ 450 nm pump wavelength with upward arrows. The emission in the yellow region in ZBLAN glass is shown by the downward arrows. The yellow light ESA is shown by the upward dashed line.

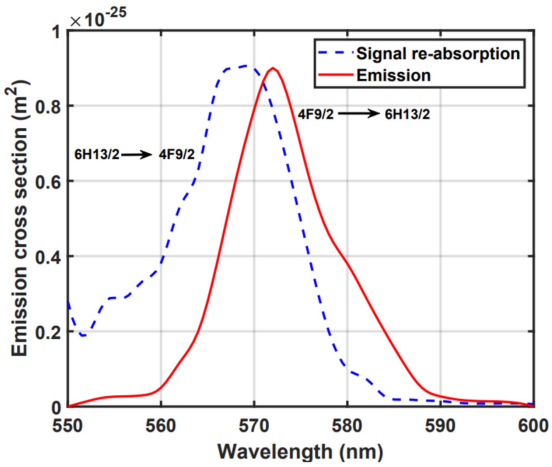

Fig. 2. Emission and signal re-absorption cross-sections of two lasing levels, ${}^4F_{9/2} \leftrightarrow {}^6H_{13/2}$ for the Dy^{3+} ion, extracted from the literature [19].

The absorption and emission spectra of the Dy−doped fiber have been obtained starting from the experimental data reported in [18], [19]. In particular, the absorption, emission, and re-absorption cross-sections were obtained by using a cubic method [27] initialized in MATLAB. The spectra used in the simulations are shown in Fig. 2. In the numerical simulations, the absorption, emission, and re-absorption cross-sections were considered in the wavelength range of 550–600 nm with a step of 0.5 nm. The yellow light re-absorption cross-section has been considered in the simulations to take into account the signal ESA effect on lasing performance.

As it is well-known, a cavity is needed to have a gain medium and laser emission. The active fiber between the reflecting mirrors as shown in Fig. 3, composes the cavity and the mirrors on the left and right sides, provide feedback at the lasing wavelength.

As it has been illustrated in Fig. 3, the pump with an input power of $P_P = 450$ mW is launched into the Dy−doped fiber core with a core diameter $d_{core} = 12.5$ μm and the numerical aperture NA = 0.16. These parameters guarantee single-mode

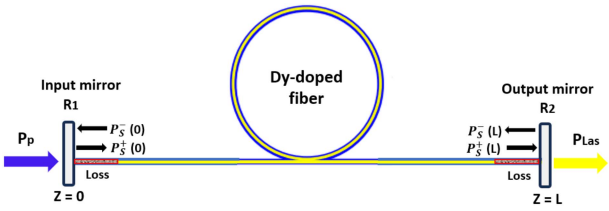

Fig. 3. Schematic of the fiber laser setup. $P_s^+(z)$ and $P_s^-(z)$ are forward and backward signal power propagating respectively in the positive and negative Z direction.

TABLE I
STRUCTURAL AND PHYSICAL PARAMETERS OF THE INVESTIGATED DY−DOPED ZBLAN FIBER LASER

Structural and Physical Parameters	Value
NA	0.16
d_{core}	12.5 μm
doping concentration, N_t	3.66×10^{25} m^{-3}
fibre length, L	4 m
background loss	0.18 dB/m
R_1	90 %
R_2	50 %
λ_p	450 nm
λ_s	573 nm
σ_{abp}	0.64×10^{-25} m^2
σ_{abs}	0.70×10^{-25} m^2
σ_{ems}	0.90×10^{-25} m^2
Γ_p	0.70
Γ_s	0.65
τ_{32}	100×10^{-6} s
τ_{21}	1.5×10^{-3} s
τ_{30}	0.01 s
τ_{10}	650×10^{-6} s

operation from 2.6 μm, so, the fiber is multi-mode for both the pump and the lasing wavelengths (450 nm and 573 nm). Higher-order modes can thus be excited in the fiber core. This also affects the values of the pump and signal overlap integrals with the doped region Γ_p and Γ_s respectively. The values of 0.70 and 0.65 chosen here for Γ_p and Γ_s have been obtained by using a modal solver based on the Finite Element Method (FEM) [28]. These values are in agreement with the corresponding values in other works [29]. The radiative lifetime values of τ_{21} and τ_{10} related to the respective energy levels $^4F_{9/2}$ and $^6H_{13/2}$ are 1.5 ms and 0.65 ms [19]. On the other hand the nonradiative lifetime values of τ_{32} and τ_{30} are estimated to be respectively 100×10^{-6} s and 0.01 s. $A_{30} = 1/\tau_{30}$ indicates the spontaneous decay rate at the pump wavelength. It should be mentioned that the nonradiative lifetime τ_{32} is much lower than that of τ_{21} one, related to the long-lived lasing level ($^4F_{9/2}$). The parameters of the system have been reported in Table I.

As expressed in Table I, σ_{abp} is the absorption cross section at the pump wavelength λ_p, σ_{abs} and σ_{ems} are the reabsorption and emission cross sections at the signal wavelength $\lambda_s = 573$ nm, τ_{32}, τ_{21}, τ_{30}, and τ_{10} are the energy level lifetimes. The parameters R_1 and R_2 are the reflectivities of input and output mirrors for the signal (laser) wavelength. Both mirrors are considered to be transparent at the pump wavelength.

III. NUMERICAL ANALYSIS

Developing fiber laser systems relying on only experimental work can be inefficient. Additionally, the current progress of fiber lasers requires accurate numerical modeling of the system. Choosing the suitable numerical model is advantageous because it provides not only an understanding of the system under investigation but one can also conduct a wide range of experiments to optimize the device's design and foresee its limitations. In other words, using a good model helps to predict the behavior of the characteristics of the fiber laser without performing experiments, which can sometimes be difficult to carry out in the laboratory. Analysis and simulation of the fiber laser systems require the solution of two groups of equations. The first group is the rate equations of the active medium, which describes the distributions of population inversion. The second group of equations is the propagation equations, consisting of several coupled non-linear first-order ordinary differential equations (ODEs) which describe the propagation of the optical fields inside the cavity. The analytical solutions of these equations are usually complicated to find. Therefore, we have to resort to a numerical method to solve these equations. Here, the FTCS technique which is an approach based on the finite-difference time-domain (FDTD) method is chosen to simulate the system. This numerical method is particularly convenient for evaluating transient problems. Additionally, the FDTD is quite versatile, and given the present computer technology, it has been used with great success in solving many practical problems [26]. Particularly this method is also applicable in the case of a pulsed Dy−doped fiber laser.

A. Rate Equations

As can be seen in Fig. 1, a four-level system is considered with a ground state $^6H_{15/2}$ denoted by 0, the highest state $^4I_{15/2}$ labeled 3 (into which energy is pumped), and states 1 ($^6H_{13/2}$) and 2 ($^4F_{9/2}$), which are lower and upper lasing transition, respectively. The upper lasing level often has a long lifetime in the case of efficient lasers and amplifiers. Hence, it is sometimes referred to as the meta-stable level. The populations of the levels are labeled N_0, N_1, N_2, and N_3. Experimental investigations have demonstrated the existence of ESA from the lower laser level. In the numerical model, the signal reabsorption cross-sections are used to assess the impact of ESA. Here we have considered the transitions that are important for the yellow-light emission process. To obtain lasing, we need a population inversion between the involved states 1 and 2. According to the electronic transition process of the four-level system of Dy, shown schematically in Fig. 1, the populations of different energy levels are expressed by the following rate equations

$$\frac{dN_0}{dt} = -W_{03}N_0 + (W_{30} + A_{30})N_3 + A_{10}N_1 \quad (1)$$

$$\frac{dN_1}{dt} = (W_{21} + A_{21} + W_{21f} + W_{21b})N_2 - A_{10}N_1 - (W_{12} + W_{12f} + W_{12b})N_1 \quad (2)$$

$$\frac{dN_2}{dt} = -(W_{21} + A_{21} + W_{21f} + W_{21b})N_2 + A_{32}N_3 + (W_{12} + A_{12} + W_{12f} + W_{12b})N_1 \quad (3)$$

$$\frac{dN_3}{dt} = W_{03}N_3 - (W_{30} + A_{30})N_3 + A_{32}N_3 \quad (4)$$

TABLE II
COEFFICIENTS USED IN THE SYSTEM OF (1)–(6)

Parameter	Definition	Relation
W_{03}	Pump absorption rate at λ_p	$\frac{\sigma_{03}P_p}{h\nu_p}$
W_{30}	Stimulated emission rate at λ_p	$\frac{\sigma_{30}P_p}{h\nu_p}$
A_{30}	Spontaneous emission rate from level 3	$\frac{1}{\tau_{03}}$
A_{10}	Spontaneous emission rate from level 1	$\frac{1}{\tau_{10}}$
W_{21}	Stimulated emission rate at λ_s	$\frac{\sigma_{21}P_s}{h\nu_s}$
A_{21}	Spontaneous emission rate from level 2	$\frac{1}{\tau_{21}}$
W_{21f}	Stimulated emission rate at λ_{ASEF}	ASETerm(λ_i, σ_{21})
W_{21b}	Stimulated emission rate at λ_{ASEb}	ASETerm(λ_i, σ_{21})
W_{12}	Absorption rate at λ_s	$\frac{\sigma_{12}P_s}{h\nu_s}$
W_{12f}	Absorption rate at λ_{ASEF}	ASETerm (λ_i, σ_{12})
W_{12b}	Absorption rate at λ_{ASEb}	ASETerm (λ_i, σ_{12})

In a steady-state situation, the time derivatives will all be zero,

$$\frac{dN_0}{dt} = \frac{dN_1}{dt} = \frac{dN_2}{dt} = \frac{dN_3}{dt} = 0 \tag{5}$$

and the total population N_t is given by

$$N_t = N_0 + N_1 + N_2 + N_3 \tag{6}$$

Under these constraints and after algebraic manipulation of the system of (1)–(6), the population of levels can be written as

$$N_1 = \frac{ce - bf}{ae - bd} \tag{7}$$

$$N_2 = \frac{af - cd}{ae - bd} \tag{8}$$

where the coefficients of a, b, c, d, e, and f are respectively $(W_{12} + W_{12f} + W_{12b} + A_{10})$, $(W_{21} + A_{21} + W_{21f} + W_{21b})$, 0, $\frac{(W_{30}+A_{30}+A_{32}+W_{03})A_{10}}{W_{03}A_{32}}$ + 1, 1, and 1. Various coefficients used in the system of (1)–(6) are defined in Table II.

In Table II, P represents the power (for the pump, signal, or amplified spontaneous emission), $\sigma_{12(21)}$ is the absorption (or emission) cross-section between energy levels 1 and 2 (2 and 1), h is the Planck constant and ν is the frequency of the radiation.

B. Power Propagation Equations

The power propagation equations describe the evolution of the pump, signal or laser radiation, and ASE radiations along the active fiber. For a systematic formulation, the wavelength spectrum is divided into slots, and in each slot, the evolution of these quantities along the z-direction is determined by a set of coupled first-order differential equations as follows:

$$\frac{dP_p}{dz} = -\Gamma_p\sigma_{03}N_0P_{0p} + \Gamma_p\sigma_{30}N_3P_{0p} - \alpha P_{0p} \tag{9}$$

$$\frac{dP_s}{dz} = -\Gamma_s\sigma_{12}N_1P_{0\,s} + \Gamma_s\sigma_{21}N_2P_{0\,s} - \alpha P_{0\,s} + ASETerm(\lambda_s)\frac{N_2}{N_t} \tag{10}$$

$$\frac{dP_{ASEF}}{dz} = -\Gamma_s\sigma_{12}N_1P_{ASEF} + \Gamma_s\sigma_{21}N_2P_{ASEF} - \alpha P_{ASEF} + ASETerm(\lambda_{ASEF})\frac{N_2}{N_t} \tag{11}$$

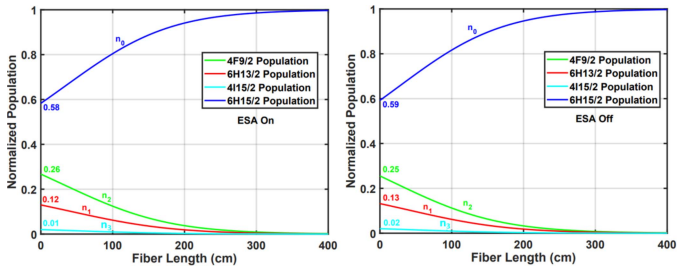

Fig. 4. Normalized population distribution ($n_j = N_j/N_t$, j = 0–3) as a function of Dy−doped fiber length, (left) including the signal re-absorption (ESA on) and, (right) ignoring the ESA (ESA off), under the pump power of 450 mW.

$$\frac{dP_{ASEB}}{dz} = -\Gamma_s\sigma_{12}N_1P_{ASEB} + \Gamma_s\sigma_{21}N_2P_{ASEB} - \alpha P_{ASEB} + ASETerm(\lambda_{ASEB})\frac{N_2}{N_t} \tag{12}$$

where ASETerm represents the amplification rate for spontaneous emission of all wavelengths in the radiation spectrum (550–600 nm). ASETerm mentioned in Table II as well, is given by the function of $\frac{2\Delta\lambda\Gamma_s\sigma_{12(21)}hc^2}{\lambda_i^3}N_t$. Furthermore, Γ_p and Γ_s represent the overlap integrals between pump radiation, signal or lasing light, and active-ion distribution. A detailed definition of these parameters can be found in [30].

Having solved (1)–(12) with solutions written in (7)–(8), and coefficients presented in Table II, the normalized population distributions ($n_j = N_j/N_t$, j = 0–3) for all appropriate yellow laser levels have been calculated by the FTCS method as a function of fiber length. Results have been shown in Fig. 4 when the population inversion between the lasing levels of $^4F_{9/2}$ and $^6H_{13/2}$, along the fiber length is observable. Notice that the normalized population of $^4F_{9/2}$ level that is $n_2 = N_2/N_t$, in the case of ESA is slightly higher than the one when ignoring the ESA. Consequently regarding the coupled transitions among the other three levels, their population in the case of ESA is slightly decreased compared with the one ignoring the ESA. Furthermore, since the energy level $^4I_{15/2}$ is strongly non-radiatively coupled to the neighboring lower level of $^4F_{9/2}$, the population is not significant.

Secondly, by solving the system of (1)–(12) by FTCS method, the pump and signal power evolution considering the impact of ESA has been computed as shown in Fig. 5. It can be seen that when ESA is considered, the signal power is amplified by the Dy−doped yellow fiber and reaches $\sim$ 148 mW from 107 mW. On the other hand, by ignoring the ESA (ESA off in Fig. 5), further amplification of the signal at the end of the fiber is observed (reaching $\sim$173 mW from 107 mW at the beginning of fiber). Additionally, it is evident that pump output power is partially higher or pump absorption decreases slightly when ESA is considered. This can be interpreted by analyzing the population evolution in the long-lived $^4F_{9/2}$ and $^6H_{13/2}$ levels. Because of the re-absorption of the intracavity yellow light from the excited level $^6H_{13/2}$, the population in the upper $^4F_{9/2}$ lasing level increases. This leads to less effective pump absorption and slightly higher pump power at the end of the fiber.

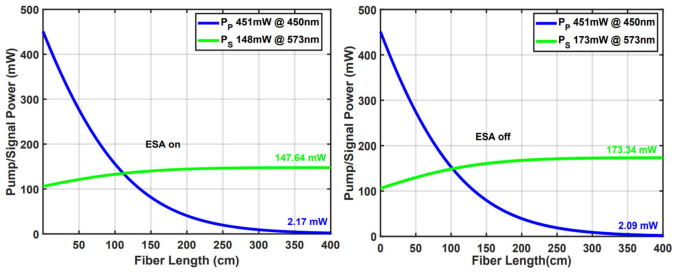

Fig. 5. Pump and signal power evolution along the Dy−doped fiber for a forward propagation signal with an input power of 107 mW, (left) considering the signal re-absorption (ESA on), and (right) without considering the ESA (ESA off).

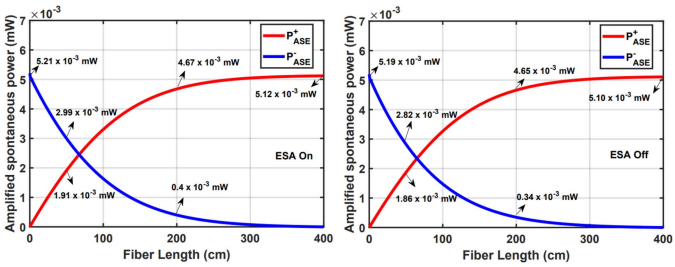

Fig. 6. Forward and backward ASE power (respectively shown as P^{+}_{ASE} and P^{-}_{ASE}) evolution along the Dy−doped fiber for a forward propagation signal with an input power of 107 mW, (left) considering ESA, and (right) without considering the ESA.

The higher output signal power in case of ignoring the ESA is due to its role as a source of loss. In other words, ESA occurs when an ion in the long-lived level is promoted to a higher energy one by absorbing either a pump or signal photon. The ion then returns to the long-lived level or ground-state levels through phonon interactions and spontaneous emission so that ESA results in an effective loss [31]. It should be mentioned that the laser output power is calculated by multiplying the signal output power at the end of the fiber and the output mirror transmission. Since the output mirror reflectivity at signal wavelength is 50%, the output laser power in the case of the first example expressed above is calculated to be ∼74 mW and 86.5 mW respectively with and without considering the ESA. It is worth mentioning that the calculated laser power of 74 mW here is in good agreement with the experimentally measured output power for a similar fiber laser investigated in [19].

We further analyzed ASE both in forward and backward directions. This parameter in the presence and absence of ESA has been calculated in the wavelength spectrum (550–600 nm). The results in the case of the signal wavelength of Fig. 5 have been shown in Fig. 6 which demonstrated that ESA has a partial effect on ASE power. Both the forward and backward ASE powers slightly decrease in case of ignoring ESA.

This is interpretable since including the ESA increases the population in the upper $^4F_{9/2}$ lasing level. This, in turn, causes more ions available in the upper lasing level for ASE. In Fig. 6, in three different positions along the fibre $L = 0.5$, 2, and 4 m, the P^{+}_{ASE} and P^{-}_{ASE} have been compared. Decreasing the powers in case of ignoring the ESA is observable. In Fig. 7 the distribution

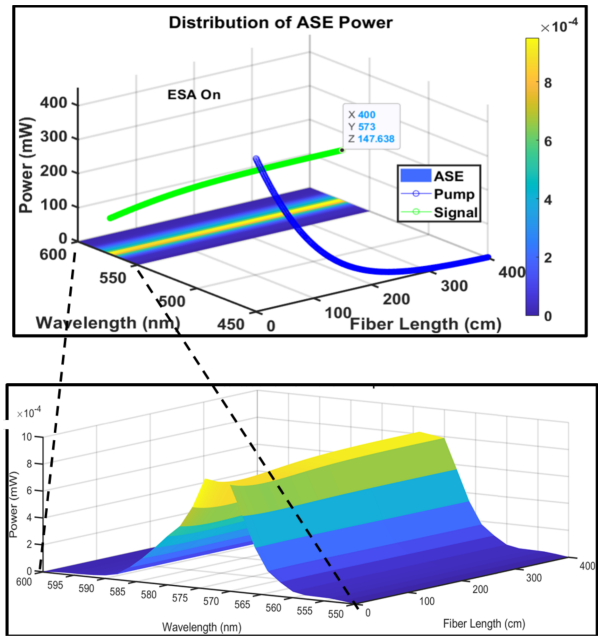

Fig. 7. Distribution of the pump, signal, and ASE powers in terms of the wavelength and fiber length considering the ESA.

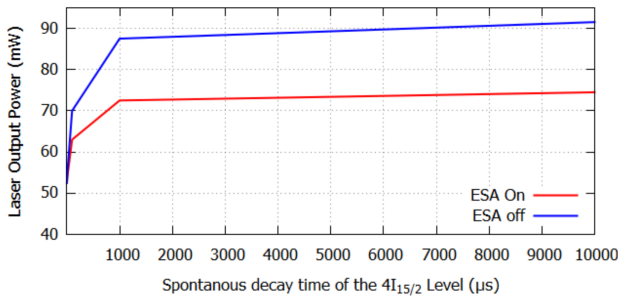

Fig. 8. Output laser power in terms of the spontaneous decay time of the $^4I_{15/2}$ level.

of the ASE, signal, and pump powers along the fiber length in all the emission wavelength ranges of 550–600 nm, has been illustrated. It should be mentioned that the signal and pump power evolution in Fig. 7 is consistent with the one in Fig. 5.

Finally, the FTCS model is employed to evaluate the effect of lifetime value changes in the four-level system of the Dy $^{3+}$− fiber laser. Our simulations show that the two most affecting lifetimes in the laser performance are τ_{30} and τ_{10}. Firstly the spontaneous decay time of the $^4I_{15/2}$ level at the pump wavelength, τ_{30}, is changed from 1 μs to 10^5 μs in two different conditions with and without ESA. The impact of τ_{30} on laser output power has been illustrated in Fig. 8. It can be seen that changing τ_{30} from 1 μs to 1000 μs causes an abrupt increase in the output power (from 52.5 mW to 72.5 mW). This is due to the decreasing spontaneous decay rate A_{30} and therefore the laser output performance improves. It's worth mentioning that this power-increasing prediction is just based on theoretical investigation. However, for τ_{30} higher than 1000 μs, the output power is slightly increasing. By increasing τ_{30} from 1000 μs to 10000 μs, the output power changes from 72.5 mW to

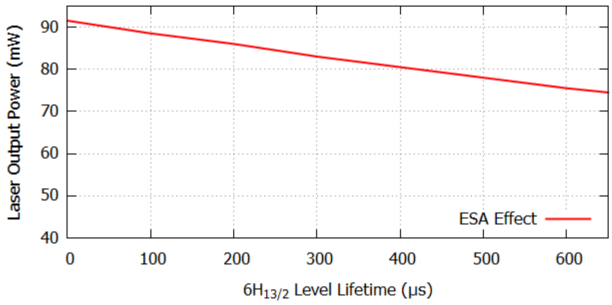

Fig. 9. Output laser power in terms of the spontaneous decay time of the ${}^6H_{13/2}$ level.

74.5 mW. A further increase of τ_{30} to 10^5 μs will cause an output power increment lower than 0.5 mW. This confirms that the initial estimation of $\tau_{30} = 10^4$ μs in our previous calculations is reasonable and reliable. In other words, for $\tau_{30} > 10^4$ μs, the output power increase is negligible, which means that this parameter is no longer affecting the laser performance. It should be mentioned that the observed behavior in output power in terms of τ_{30} changes, in the case of neglecting ESA is the same as in the case with ESA. However, by neglecting the ESA, all the powers are shifted to a higher value.

We also considered the effect of ESA on the laser output power laser. We decreased the τ_{10} value from 650 μs to 10^{-5} μs. At the lowest value of $\tau_{10} = 10^{-5}$ μs, the highest output laser power of 91.5 mW is obtained. Results have been shown in Fig. 9. Notice that, by decreasing the lower laser level ${}^6H_{13/2}$ lifetime (τ_{10}), a higher output laser power is observed. Indeed, decreasing the τ_{10} value which is equivalent to reducing the impact of the ESA, will cause a faster depopulation of the lower level of the yellow laser transition (${}^6H_{13/2}$), and consequently a higher pumping to the ${}^4I_{15/2}$ level and a higher laser output power. The same effect of decreasing τ_{10} in real conditions can be obtained by designing a cascade lasing arrangement in which the lower laser level of yellow transition is employed as the upper laser level of the mid-infrared one [19].

IV. Output Efficiency of the Laser

A critical parameter of an optically pumped laser is its slope efficiency η, which is defined as the slope of the curve obtained by plotting the laser output power P_{Las}, versus the pump power. To find the efficiency of the laser, first, we need to find the pump power threshold. At this power, the laser threshold is just reached, usually assuming steady-state conditions, and the small signal gain equals the losses of the laser cavity. Finally, the output power of the laser with threshold pump power P_{th} can be calculated for a given pump power P_p (above that threshold) as follows

$$P_{Las} = \eta(P_p - P_{th}) \tag{13}$$

Finding P_{th} can be approximately performed by analytical expressions. Here for obtaining P_{th} for the four-level system of a Dy − fiber laser, we used the analytical method described in [31]. With this approach P_{th} is obtained by using the intrinsic saturation powers, and the cross-saturation powers at the pump

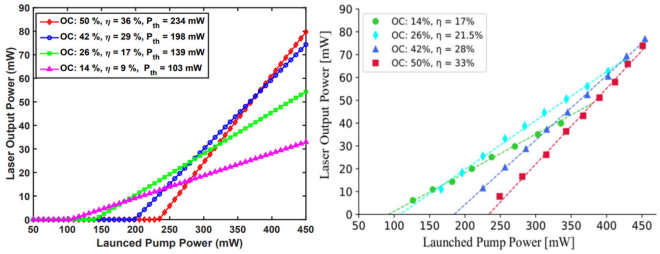

Fig. 10. Yellow laser output power as a function of launched pump power at different output couplers (left) simulated here, and (right) experimentally obtained in [19].

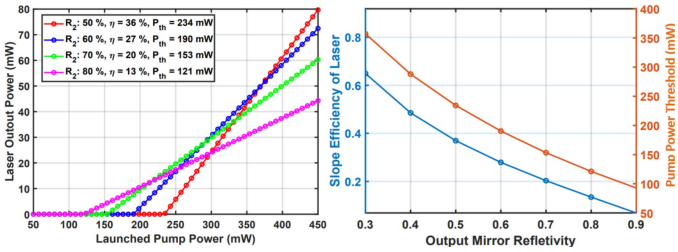

Fig. 11. (left) Yellow laser output power as a function of launched pump power at different output mirror reflectivity of 50–80 % and (right) calculated values of slop efficiency and pump power threshold at reflectivity range of 30–90% [19].

and laser wavelengths. To verify the correctness of this analytical method, we analyzed output power efficiency and pump threshold for different R_2 similar to the experimental research in [19]. Therefore, different values of output mirror reflectivity $R_2 = 50\%, 58\%, 74\%, 86\%$ equivalent to output coupler OC values respectively $OC = 50\%, 42\%, 26\%$, and 14%, have been chosen. The simulated laser slope efficiencies and thresholds with the mentioned values of R_2 (as shown in Fig. 10) have been calculated which are in good agreement with their equivalent values experimentally obtained in [19].

A. Mirror Reflectivity

To accurately evaluate the impact of different structural and physical parameters on the performance of the laser, and to find the configurations providing the maximum possible slope efficiency, optimization simulations have been performed. In our simulations, the realistic values reported in Tables I and II are considered. Firstly we have changed the output mirror reflectivity from $R_2 = 30\%$ to $R_2 = 90\%$, while other parameters are fixed, that is $\Gamma_s = 0.65$, $\Gamma_p = 0.70$ and $L = 4$ m. In Fig. 11, the laser slope efficiency η and pump power threshold P_{th} versus the output mirror reflectivity R_2 are shown. As it is observable in Fig. 11, the laser efficiency has the maximum values ($\eta \sim 65\%$), for the mirror reflectivity $R_2 = 30\%$. However, at this value of R_2, the P_{th} is relatively high ($P_{th} = 357$ mW).

B. Overlap Integrals

We also simulated laser slope efficiencies and thresholds for different values of signal or lasing (Γ_s) and pump (Γ_p) overlap integrals. Since the fiber simulated here is multimode for both the laser and pump wavelength, different lasing and

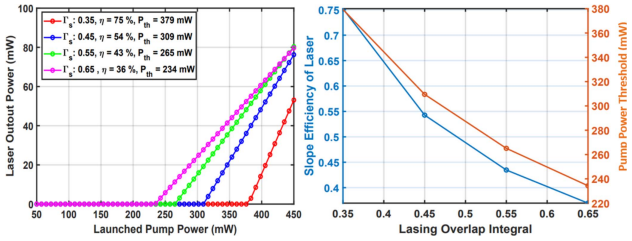

Fig. 12. (left) Yellow laser output power as a function of launched pump power at different lasing overlap integrals of 0.35–0.65 and (right) calculated values of slop efficiency and pump power threshold at different lasing overlap integrals of 0.35–0.65.

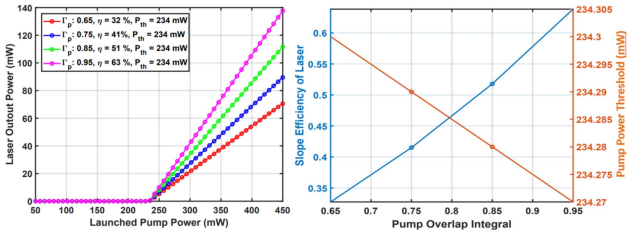

Fig. 13. (left) Yellow laser output power as a function of launched pump power at different pump overlap integrals of 0.65–0.95 and (right) calculated values of slop efficiency and pump power threshold at different pump overlap integrals of 0.65–0.95.

pump modes with different values of overlap integrals might be used in the lasing process. It's worth mentioning that the values $\Gamma_s = 0.65$ and $\Gamma_p = 0.70$ used for the simulation have been obtained by testing different possible sets of Γ_s and Γ_p calculated using a finite-difference approach implemented in python as well as FEM modal solver. The chosen values of Γ_s and Γ_p provide the highest matching with experimental results reported in [29] and [18]. In this analysis, we have examined the effect of changing Γ_s or Γ_p and the impact on laser efficiency and pump power threshold. Results obtained by changing Γ_s and Γ_p have been illustrated in Figs. 12 and 13. First, we calculated slope efficiencies and thresholds at a fixed amount of $\Gamma_p = 0.70$ and a changing amount of Γ_s in the range 0.35–0.65. Second, we calculated slope efficiencies and thresholds at a fixed amount of $\Gamma_s = 0.65$ and a changing amount of Γ_p in the range 0.65–0.95. It should be mentioned that in these simulations the parameters of R_1, R_2, and L are fixed at respectively, 90%, 50%, and 4 m.

C. Active Fiber Length

Finally, we evaluate the impact of different active fiber lengths being the fiber active cavity medium, on the laser output performance. As can be seen in Fig. 14, fiber length is changed from 0.5 m to 4 m while other parameters are fixed at $\Gamma_s = 0.65$, $\Gamma_p = 0.70$, $R_1 = 90\%$, and $R_2 = 50\%$. We figured out that the maximum achievable slope efficiency is $\eta \sim 78\%$ for the fiber length $L = 8.5$ m.

V. Discussion

The performance of a Dy−doped fiber laser with yellow emission at 573 nm has been analyzed. The Dy−doped fiber simulated here has the same structural parameters as the

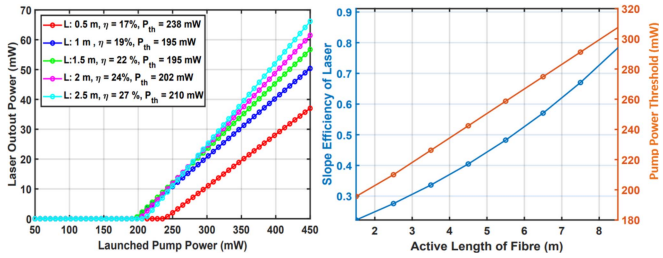

Fig. 14. (left) Yellow laser output power as a function of launched pump power at different active fiber lengths of 0.5–2.5 m and (right) calculated values of slop efficiency and pump power threshold at active fiber lengths of 1.5–8.5 m.

commercially available Dy−doped fiber made by the Le Verre Fluoré, France [24]. Two different numerical and analytical approaches are chosen to fully understand the different transitions involved in the lasing mechanism of the fiber and their impact on the laser output performance. Having solved the rate and propagation equations in a four-level Dy−doped fiber laser by the FTCS method, the effect of ESA and ASE on the output power of the laser has been figured out. ESA has a significant impact on the laser performance. By increasing the transition rate A_{10}, the ESA impact on laser output power is decreased. As can be seen in Fig. 8, decreasing τ_{10} from 650 μs to 10^{-5} μs, provides an increase of the output power from 74.5 mW to 91.5 mW. Then, further possible changes in laser output power have been predicted by changing the transition rate A_{30} in the fiber laser system. For τ_{30} values higher than 1000 μs, the effect of the pump spontaneous decay will be negligible. Hence the output laser power slightly changes.

In Fig. 10–14, pump threshold and laser slope efficiency changes are examined under the variation of four different parameters, that is R_2, Γ_s, Γ_p, and L. First, the pump threshold and slope efficiency have been calculated in the R_2 range 30–90% with a step of 10%. Decreasing the output mirror reflectivity from 50% to 30%, the slope efficiency has increased from 36% to 65%. However, the pump power threshold has been also increased from 234 mW to 357 mW which is not desirable. Secondly, we have calculated the output power of the laser, slope efficiency, and its threshold by changing the Γ_s and Γ_p in the ranges respectively 0.35–65 and 0.65–0.95 by a step of 0.10. Similar to the impact of R_2, reducing the lasing overlap integral to 0.35 has provided a high slope efficiency of 75% and an increased pump threshold of 379 mW. On the other hand, increasing the Γ_p from 0.70 to 0.95 will increase the slope efficiency to 63%, and the pump threshold remains as low as 234 mW. Nevertheless, the Γ_s and Γ_p parameters for the chosen parameters of the Dy−doped fiber simulated here, can not be far apart. In other words, comprise condition of high efficiency and low pump power threshold, can occur at a range of 0.65–0.85 for both the Γ_s and Γ_p. Finally by increasing the active fiber length to 8.5 m, the highest η of 78% is achieved while the pump threshold is still relatively low (307 mW). It is worth mentioning that increasing the active fiber length to the range of 4.5–8.5 m could obtain optimized performance of fiber laser with a trade-off between the high output efficiency and low pump power threshold. In this range of fiber length slope efficiencies,

more than half of the Stokes limit (of 78%) in the range of 40–78% are predicted with low pump power thresholds in the range of 242–307 mW.

VI. Conclusion

The FTCS numerical method and the analytical approach have been developed to fully evaluate the performance of the Dy−doped fiber laser. Two sources of loss ESA and ASE have been taken into account in the model. The influence of the ESA loss on laser output power can be significantly reduced by decreasing τ_{10} to 10^{-5} μs. Exploiting the developed analytical approach for the four-level system of Dy−doped fiber laser, the impact of fiber cavity parameters on the slope efficiency and pump power threshold was investigated. Optimized criteria for finding the Dy−doped yellow fiber lasers with high efficiency have been found. The found criteria are output mirror reflectivities less than 50%, lasing overlap integrals less than 0.65, pump overlap integrals higher than 0.75, and finally, fiber length more than 4.5 m, to obtain $\eta \geq 36\%$. The value of efficiency reported here is higher than other reported values for the efficiency of the same fiber [18], [19]. Additionally, the fiber length parameter is the most effective in achieving efficient Dy−doped fiber yellow fiber lasers. Choosing the active fiber length in the range of 4.5–8.5 m could obtain optimized performance of fiber laser with a trade-off between the high output efficiency and low pump power threshold. In this range of fiber length, slope efficiencies more than half of the Stokes limit, in the range of 40–78% are predicted with low pump power thresholds in the range of 242–307 mW.

References

[1] D. Lavinsky et al., "Nondamaging retinal laser therapy: Rationale and applications to the macula," *Invest. Ophthalmol. Vis. Sci.*, vol. 57, no. 6, pp. 2488–2500, 2016.

[2] L. Zhang, H. Jiang, S. Cui, J. Hu, and Y. Feng, "Versatile Raman fiber laser for sodium laser guide star," *Laser Photon. Rev.*, vol. 8, no. 6, pp. 889–895, 2014.

[3] K. Aflalo, M. Ben-David, A. Stern, and I. Juwiler, "Theoretical investigation of using a yellow (577 nm) laser for diabetic retinopathy," *OSA Continuum*, vol. 3, no. 11, pp. 3253–3266, 2020.

[4] T. Hong, C. Cramer, E. Cook, W. Nagourney, and E. Fortson, "Observation of the 1S0-3P0 transition in atomic ytterbium for optical clocks and qubit arrays," *Opt. Lett.*, vol. 30, no. 19, pp. 2644–2646, 2005.

[5] N. Kapany, N. Peppers, H. Zweng, and M. Flocks, "Retinal photocoagulation by lasers," *Nature*, vol. 199, pp. 146–149, 1963.

[6] T. Verdina et al., "The role of subthreshold micropulse yellow laser as an alternative option for the treatment of refractory postoperative cystoid macular edema," *J. Clin. Med.*, vol. 9, no. 4, 2020, Art. no. 1066.

[7] D. Coutts, M. Ainsworth, and J. Piper, "Efficient green/yellow conversion of copper vapour laser output," *Opt. Commun.*, vol. 75, no. 3/4, pp. 301–306, 1990.

[8] J. Ota, A. Shirakawa, and K.-I. Ueda, "High-power yb-doped double-clad fiber laser directly operating at 1178 nm," *Japanese J. Appl. Phys.*, vol. 45, no. 2L, 2006, Art. no. L117.

[9] E. M. Dianov, A. V. Shubin, M. A. Melkumov, O. I. Medvedkov, and I. A. Bufetov, "High-power CW bismuth-fiber lasers," *J. Opt. Soc. Amer. B*, vol. 24, no. 8, pp. 1749–1755, 2007.

[10] M. Fallahi et al., "5-W yellow laser by intracavity frequency doubling of high-power vertical-external-cavity surface-emitting laser," *IEEE Photon. Technol. Lett.*, vol. 20, no. 20, pp. 1700–1702, Oct. 2008.

[11] J. Limpert, H. Zellmer, P. Riedel, and A. Tünnermann, "Laser oscillation in yellow and blue spectral range in Dy^{3+}: ZBLAN," in *Proc. Conf. Lasers Electro- Opt.*, 2001, Art. no. CWJ4.

[12] M. C. Falconi et al., "Dysprosium-doped chalcogenide master oscillator power amplifier (MOPA) for Mid-IR emission," *J. Lightw. Technol.*, vol. 35, no. 2, pp. 265–273, Jan. 2017.

[13] M. C. Falconi et al., "Design of an efficient pumping scheme for mid-IR Dy^{3+}:Ga_5 $Ge_{20}Sb_{10}$ S_{65} PCF fiber laser," *IEEE Photon. Technol. Lett.*, vol. 28, no. 18, pp. 1984–1987, Sep. 2016.

[14] P. Paradis et al., "Dysprosium-doped silica fiber as saturable absorber for mid-infrared pulsed all-fiber lasers," *Opt. Exp.*, vol. 30, no. 3, pp. 3367–3378, 2022.

[15] Y. Fujimoto, O. Ishii, and M. Yamazaki, "575 nm laser oscillation in Dy-doped waterproof fluoro-aluminate glass fiber pumped by violet GAN laser diodes," in *Proc. SPIE*, vol. 7912, pp. 152–158, 2011.

[16] S. Bowman, S. O'Connor, and N. Condon, "Diode pumped yellow dysprosium lasers," *Opt. Exp.*, vol. 20, no. 12, pp. 12906–12911, 2012.

[17] G. Bolognesi et al., "Yellow laser performance of Dy^{3+} in co-doped dy, tb: $LiLuF_4$," *Opt. Lett.*, vol. 39, no. 23, pp. 6628–6631, 2014.

[18] M. Amin, M. Majewski, and S. Jackson, "Yellow emission from dysprosium-doped ZBLAN fiber laser," in *Proc. SPIE*, vol. 11260, pp. 197–203, 2020.

[19] M. Amin, S. Jackson, and M. Majewski, "Experimental and theoretical analysis of Dy^{3+}-doped fiber lasers for efficient yellow emission," *Appl. Opt.*, vol. 60, no. 16, pp. 4613–4621, 2021.

[20] S. Tian et al., "Silicate-clad Dy^{3+}-doped multi-component phosphate glass core glass fiber for yellow laser applications," *J. Non-Crystalline Solids*, vol. 577, 2022, Art. no. 121313.

[21] A. M. Loconsole, M. C. Falconi, A. Annunziato, S. Cozic, S. Poulain, and F. Prudenzano, "Design of a Mid-IR laser based on a ho: Nd-codoped fluoroindate fiber," *J. Lightw. Technol.*, vol. 41, no. 2, pp. 702–708, Jan. 2023.

[22] F. Jobin, Y. O. Aydin, M. Bernier, and R. Vallée, "Dysprosium gain-switched fiber laser at 3.24 μm pumped at 1064 nm," *Opt. Continuum*, vol. 2, no. 2, pp. 498–505, 2023.

[23] Q. Chen et al., "Efficient and broadband emission in dy-doped glass-ceramic fibers for tunable yellow fiber laser," *Nanomaterials*, vol. 13, no. 9, 2023, Art. no. 1558.

[24] [Online]. Available: https://leverrefluore.com/products/active-fibers/re-doped-single-mode-fiber/

[25] J. Zou et al., "Direct generation of watt-level yellow dy-doped fiber laser," *Photon. Res.*, vol. 9, no. 4, pp. 446–451, 2021.

[26] J. Meyer, J. Sompo, and S. Von Solms, *Fiber Lasers: Fundamentals with MATLAB Modelling*. Boca Raton, FL, USA: CRC Press, 2022.

[27] Y.-G. Zhao and Z.-H. Lu, "Cubic normal distribution and its significance in structural reliability," *Struct. Eng. Mechanics*, vol. 28, no. 3, pp. 263–280, 2008.

[28] A. Cucinotta, F. Poli, S. Selleri, L. Vincetti, and M. Zoboli, "Amplification properties of Er-doped photonic crystal fibers," *J. Lightw. Technol.*, vol. 21, no. 3, pp. 782–788, Mar. 2003.

[29] M. Z. Amin, M. R. Majewski, R. I. Woodward, A. Fuerbach, and S. D. Jackson, "Novel near-infrared pump wavelengths for dysprosium fiber lasers," *J. Lightw. Technol.*, vol. 38, no. 20, pp. 5801–5808, Oct. 2020.

[30] S. Selleri, L. Vincetti, and A. Cucinotta, *Optical and Photonic Components*, Bologna, Italy: Società Editrice Esculapio, 2015.

[31] C. Barnard, P. Myslinski, J. Chrostowski, and M. Kavehrad, "Analytical model for rare-earth-doped fiber amplifiers and lasers," *IEEE J. Quantum Electron.*, vol. 30, no. 8, pp. 1817–1830, Aug. 1994.

Open Access funding provided by 'Università degli Studi di Parma' within the CRUI CARE Agreement